Coherent enhancement of a frequency comb modulated by a terahertz laser field in high-order harmonic generation

Yuan-Yuan Wu,[1,2] Chang-Tong Liang,[1,3] Bao-Guang Zhao,[1,2] and Peng-Cheng Li[1,2,*]

[1]*Research Center for Advanced Optics and Photoelectronics, Department of Physics, College of Science, Shantou University, Shantou, Guangdong 515063, China*

[2]*Key Laboratory of Intelligent Manufacturing Technology of MOE, Shantou University, Shantou, Guangdong 515063, China*

[3]*Institute of Applied Physics and Computational Mathematics, Beijing 100088, China*

(Received 6 January 2023; revised 5 July 2023; accepted 6 September 2023; published 2 October 2023)

We present the coherent enhancement of the frequency comb via high-order harmonic generation (HHG) in a train of infrared laser pulses combined with terahertz (THz) laser fields. The HHG spectra are obtained by solving the three-dimensional time-dependent Schrödinger equation by means of the time-dependent generalized pseudospectral method. We find that the structure of the frequency comb via HHG becomes much smoother and more regular, and the yield of the comb is increased by nearly two orders of magnitude. By analyzing the phase coherence of HHG spectra, we demonstrate that the THz laser fields are responsible for the optimization of the structure and yield of the frequency comb since the constructive phase coherence of the HHG spectra is modulated by the THz field. The physical origin of the constructive phase coherence is thanks to the uniform ionization efficiency induced by the THz laser field for each laser pulse, which greatly improves the synchronization of the harmonic emission. Our finding provides a promising method for the enhancement of the frequency comb via HHG.

DOI: 10.1103/PhysRevA.108.043101

I. INTRODUCTION

The optical frequency comb (OFC) is a kind of mode-locked pulse laser with completely locked repetition rate and phase, which has ultrahigh spatial, temporal, and frequency resolution [1]. These advantages of the OFC underlie the various applications in the fields of precision spectroscopy [2,3] and frequency measurement [4,5], such as linking optical and microwave regimes to achieve high-precision measurement of optical frequency [6–8], coherent optical storage [9], biomedical-field applications [10], and wavelength calibration of an astronomical telescope [11]. The OFC can usually be generated by mode-locked laser generation [12,13], the Kerr microcavity [14], electro-optic modulators [15], etc. In 2005, Gohle *et al.* [16] and Jones *et al.* [17] almost simultaneously pioneered the production of a coherent extreme ultraviolet (XUV) frequency comb by high-order harmonic generation (HHG) from ultrashort femtosecond laser pulses by using the femtosecond enhancement cavity. HHG is widely used as a technique for the production of XUV and vacuum ultraviolet (VUV) radiation, which can be obtained through the interaction of an ultrafast intense laser field with atoms and molecules [18,19]. A typical HHG spectrum shows a rapid drop at the first few harmonics, and then a plateau with a similar harmonic amplitude appears, followed by the cutoff harmonics with a sharp decrease in harmonic intensity. The semiclassical three-step model [20] can be used to well understand the process of HHG: the bound electrons are first released by ionization and accelerated in the applied laser field; then the electron can be driven back towards the parent ions to recombine into the ground state to emit the harmonic photons.

Recently, Yost *et al.* [21] suggested a method to generate a frequency comb via HHG below the ionization threshold in the VUV region, which has very attractive application prospects, such as probing electronic dynamics [22], electronic transitions in molecules [23], and the next-generation optical clock [24]. Kandula *et al.* [25] demonstrated the generation of a frequency comb in the XUV region and performed the first absolute frequency determination. Carrera *et al.* [26] explored in detail how the number of pulses and the laser intensity affect the frequency-comb structure generated via HHG. More recently, we reported [27] the characteristics of the structure and coherence of a frequency comb from HHG driven by laser-pulse trains when the Keldysh multiphoton ionization proceeds towards the tunneling regime. However, the way to improve the conversion efficiency of the frequency comb in the XUV band and optimize the comb structure is still an open problem. It is worth noting that terahertz (THz) pulses provide a promising way to modulate HHG combs [28–31]. THz laser pulses can be realized experimentally by optical rectification of femtosecond laser pulses [32], a photoconductive antenna [33], nonlinear optical mixing technology [34], and so on. Among them, THz pulses in the midinfrared region can be efficiently generated via difference-frequency mixing, such as two parametrically amplified pulse trains from a white-light seed.

In this work, we present the enhancement and optimization of a frequency comb via HHG by adding a series of THz

*Corresponding author: pchli@stu.edu.cn

pulses to femtosecond infrared (IR) laser fields. The HHG spectra are calculated by propagating the time-dependent Schrödinger equation (TDSE) accurately and efficiently using the time-dependent generalized pseudospectral (TDGPS) method [35]. We find that the efficiency of the frequency comb is improved thanks to the THz controlling laser pulses, and the comb structures become more regular. The prospect of our scheme provides a method for producing XUV frequency combs that satisfy the high conversion efficiency, the regular comb structure, and the broad bandwidth.

This paper is organized as follows. In Sec. II, we briefly describe our theoretical and computational methods. In Sec. III, the coherence of the frequency comb via HHG and how the THz field modulates the physical mechanism of the frequency comb are discussed. Section IV contains concluding remarks.

II. THEORETICAL METHOD

HHG can be calculated by solving the TDSE, and the TDSE can be written in the dipole approximation and length gauge as (in atomic units)

$$i\frac{\partial}{\partial t}\psi(\mathbf{r},t) = H\psi(\mathbf{r},t) = [H_0 + V(\mathbf{r},t)]\psi(\mathbf{r},t), \quad (1)$$

where H_0 is the unperturbed Hamiltonian of the hydrogen atom and $V(\mathbf{r},t)$ is the time-dependent atom-field interaction, which can be expressed as

$$V(\mathbf{r},t) = -\mathbf{E}(\mathbf{t})\cdot\mathbf{r} = -zE(t), \quad (2)$$

where $E(t)$ is composed of two pulse train as follows:

$$E(t) = E_I(t) + E_T(t), \quad (3)$$

where $E_I(t)$ and $E_T(t)$ are an IR pulse train and a THz pulse train, respectively. The fields $E_I(t)$ and $E_T(t)$ are expressed as follows:

$$E_I(t) = \sum_{n=1}^{N} E_I f_I(t-n\tau)\exp[i(\omega_I t - n\omega_I\tau + n\Delta\phi)], \quad (4)$$

$$E_T(t) = \sum_{n=1}^{N} E_T f_T(t-n\tau)\exp[i(\omega_T t - n\omega_T\tau + n\Delta\phi)], \quad (5)$$

where E_I, E_T, ω_I, and ω_T are the corresponding laser-field electric peak amplitudes and carrier frequencies of the IR train and the THz controlling train, respectively. N is the number of pulses. The pulse-to-pulse phase shift is given by $\Delta\phi$, and $f_I(t-n\tau)$ and $f_T(t-n\tau)$ are Gaussian envelope functions and can be expressed as $f(x) = \exp[-2(ln2)x^2/{\tau_0}^2]$, where τ_0 is the full width at half maximum (FWHM).

The propagation of the TDSE is performed accurately and efficiently by means of the TDGPS method in spherical coordinates. The TDGPS method takes advantage of the generalized pseudospectral technique for optimal spatial discretization of the radial coordinates in order to avoid the Coulomb singularity and maintain the long-range nature of the potential. This method makes the grid points in the near nuclear region denser and the grid points far from the nuclear region relatively sparser and can be computationally more efficient than using equal-spacing grid discretization. For atomic structure calculations, generally, the space truncates the semi-infinite $(0,\infty)$ domain into a finite domain $[r_{\min}, r_{\max}]$. So an absorber is used to filter out the wave packet reaching the outward boundary to avoid artificial reflection. We map the semi-infinite domain $[0, r_{\max}]$ to the finite domain $[-1, 1]$ using a nonlinear mapping according to Ref. [35], where $r_{\max} = 200$ a.u. and 1600 grid points are used to discretize x using the Legendre pseudospectral technique. An absorber in the form of the exponential-decay form $1/[1-\exp(br-r_0)]$ is used. Typically, we use $b = 1.25$ a.u. and $r_0 = 100$ a.u. The time propagation of the wave function is obtained with the second-order split-operator method in the energy representation [35]:

$$\psi(\mathbf{r},t+\Delta t) \simeq \exp\left(-iH_0\frac{\Delta t}{2}\right) \times \exp\left[-iV\left(\mathbf{r},t+\frac{\Delta t}{2}\right)\Delta t\right] \times \exp\left(-iH_0\frac{\Delta t}{2}\right)\psi(\mathbf{r},t) + O(\Delta t^3). \quad (6)$$

Once the time-dependent wave function $\psi(\mathbf{r},t)$ is determined, we can calculate the time-dependent induced dipole moment in the length and acceleration forms as

$$d(t) = \langle\psi(\mathbf{r},t)|z|\psi(\mathbf{r},t)\rangle, \quad (7)$$

$$d_A(t) = \langle\psi(\mathbf{r},t)|-\frac{z}{r^3}+E(t)|\psi(\mathbf{r},t)\rangle. \quad (8)$$

The HHG intensity spectra can be obtained by the Fourier transformation from the induced dipole moment in acceleration form:

$$S(\omega) = \frac{4\omega^4}{6\pi c^3}|\tilde{d}(\omega)|^2. \quad (9)$$

Here $\tilde{d}(\omega)$ is the Fourier transform of $d_A(t)$ divided by the number of pulses N to scale to the one-pulse case,

$$\tilde{d}(\omega) = \frac{1}{N\omega^2}\int_{-\infty}^{\infty} d_A(t)e^{-i\omega t}dt = \frac{1}{N}\sum_{n=1}^{N}\tilde{d}_n(\omega), \quad (10)$$

and $\tilde{d}_n(\omega)$ is the spectral dipole moment calculated by the nth dipole pulse. The spectral phase $\theta_n(\omega)$ is defined as the harmonic spectral phase of $\tilde{d}_n(\omega)$:

$$\tilde{d}_n(\omega) = |\tilde{d}_n(\omega)|e^{i\theta_n(\omega)}. \quad (11)$$

III. RESULTS AND DISCUSSION

In Fig. 1, the combined laser field composed of five successive IR laser pulses and a THz laser-pulse train is represented. For an intuitive representation, the few-cycle laser-pulse train is shown in Fig. 1, with the truncated part being the omitted time range; the laser-field parameters used are as follows: the IR laser train with laser wavelength $\lambda_I = 800$ nm and the peak intensity $I_I = 4.0\times10^{13}\,\mathrm{W/cm^2}$ are used, with a 10-fs FWHM, and the time separation between adjacent pulses is $\tau = 0.5$ ps. The THz laser pulses are generally in the spectral range between 0.3 and 30 THz [28]. Since the THz wavelength is shorter in the midinfrared region, higher peak field intensity (which is larger than 100 MV/cm) can be achieved

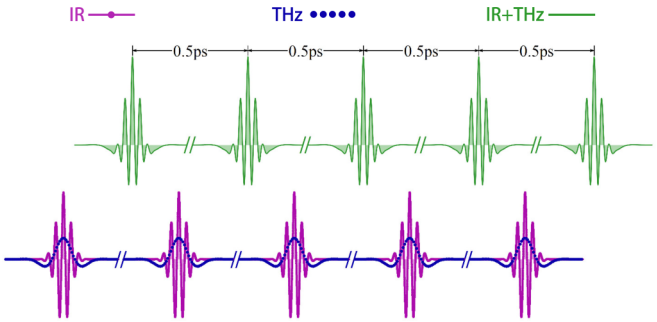

FIG. 1. The schematic of a combined laser field consisting of an IR laser-pulse train and a THz laser train is represented by the green solid line. The purple line with points and blue dotted line indicate the IR laser pulses and the THz train, respectively. The pulse train adopted in the calculation consists of five pulses with time separation $\tau = 0.5$ ps between adjacent pulses.

by tighter focusing [36,37]. The THz laser pulses with a 25-THz center frequency ($\lambda_T = 12\,000$ nm) and peak intensity $I_T = 2.5 \times 10^{12}\,\mathrm{W/cm^2}$, i.e., the peak amplitude $E_T = E_I/4 = 0.00844$ a.u., corresponds to 43 MV/cm, with a 40-fs FWHM; the other parameters used are the same as those for the IR laser field. It is convenient to set conduction-electron polarization $\Delta\phi = 0$ for the analysis of the effect of the THz field on the frequency-comb structure. It can be seen that the amplitude of the combined laser field is greatly increased compared with the original IR laser field, and the magnitude of the positive and negative components of the combined field has an obvious asymmetry due to the modulation of the THz laser pulses.

In Fig. 2, we compare the HHG spectra driven by the IR laser-pulse train alone and the combined laser-pulse train. The other laser parameters used are the same as those in Fig. 1. The purple line with points and the green solid line indicate the HHG spectra for the case of the IR laser field alone and the case of combined laser pulses, respectively, as shown in Fig. 2(a). We find that the yield of HHG spectra is significantly increased at below-threshold harmonics by adding a THz pulse train. In particular, the yield of HHG between the third-order harmonic and the fifth-order harmonics is increased by nearly two orders of magnitude. In addition, only the odd harmonics are produced for the case of the IR laser-pulse train, while even harmonics exist in the HHG spectrum driven by the combined laser train. For the

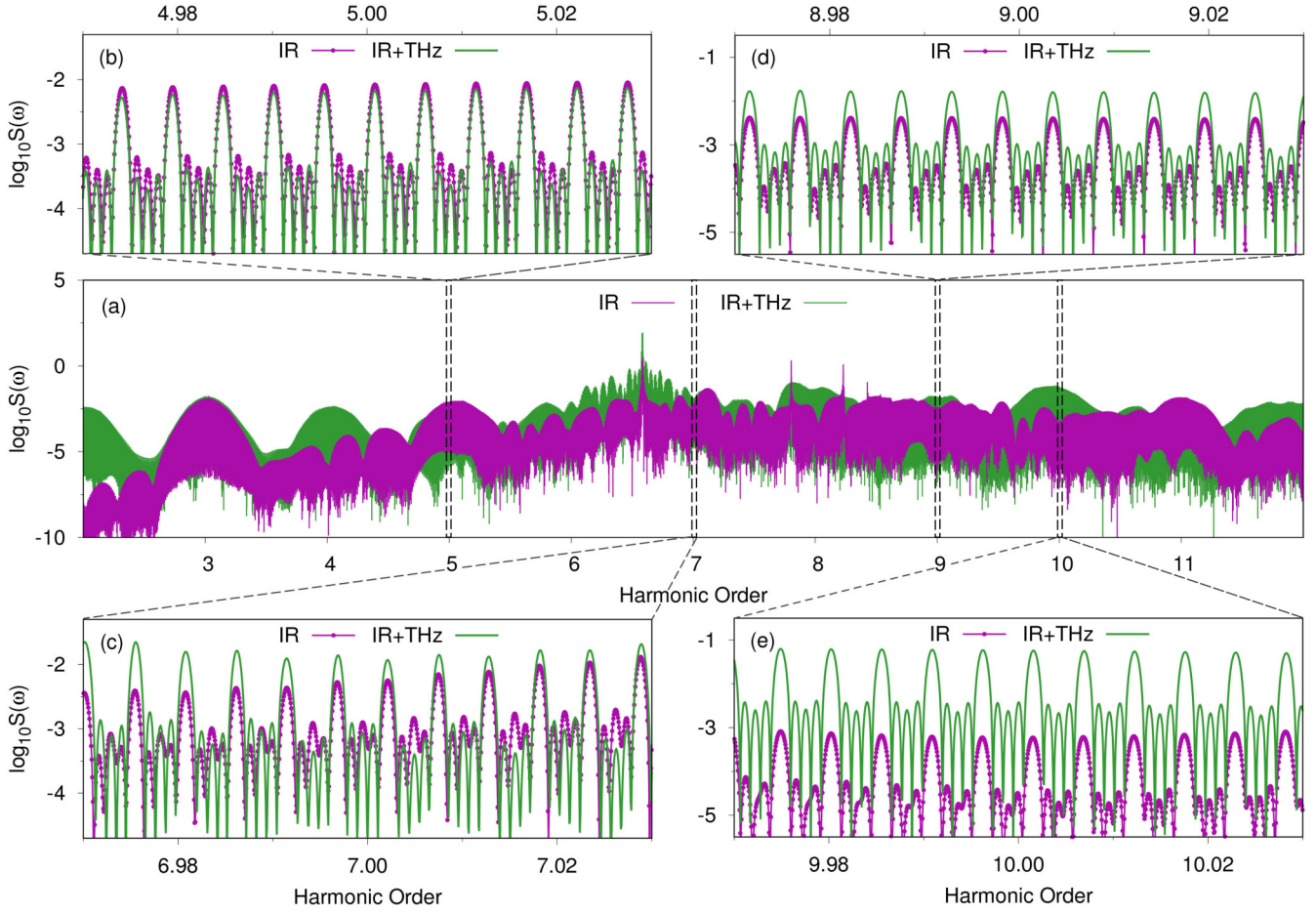

FIG. 2. (a) Comparison of the HHG spectra between the IR laser pulses alone and the combined laser-pulse train. (b)–(e) are the zoomed-in view ports of nest comb structures at below-threshold and plateau harmonics in (a), which are in the vicinity of the (b) 5th, (c) 7th, (d) 9th, and (e) 10th harmonics. The IR laser pulses have an 800-nm laser wavelength, and the peak intensity is $I_I = 4.0 \times 10^{13}\,\mathrm{W/cm^2}$. The THz pulses used are a 25-THz train with peak intensity $I_T = 2.5 \times 10^{12}\,\mathrm{W/cm^2}$.

single-atom system, assuming that the laser field is symmetric, only harmonic peaks at odd multiples of the laser frequency will appear in the spectra of HHG radiation. This is due to the fact that in a symmetric periodic laser field, the ionization, acceleration, and recombination of electrons and the emission of high-order harmonics at frequency ω occur every half laser cycle. As mentioned above, the addition of THz field greatly breaks the symmetry of the positive and negative components of the laser field, thus inducing the generation of even harmonics. To observe the fine structure of the frequency comb, we select the HHG spectra which are located at the given below-threshold and plateau harmonics and zoom in on these spectral structures, as shown in Figs. 2(b)–2(e). Figure 2(b) shows the frequency-comb structures in the vicinity of the fifth harmonic order driven by IR laser pulses and the combined laser train in detail. The lower odd-order frequency combs show almost the same intensity of the main peaks, both with three subpeaks but slightly different subpeak structures. According to previous studies [26,38], through the fully *ab initio* quantum investigation, as long as the number of pulses $N > 2$, the frequency-comb structure within each harmonic can be clearly seen. As the number of pulses N increases, the spectral width of each main-peak comb structure gradually narrows, and the number of nested subpeaks increases, with a dependence of $N - 2$ on the number of pulses. The frequency-comb subpeaks near the fifth order generated by the IR field alone show a structure with decreasing intensity. However, the frequency-comb peaks formed by the combined field show a structure that is low in the middle and high on either side. Figures 2(c) and 2(d) show detailed structure comparisons of odd-order harmonics located at below-threshold and plateau harmonics. It can be seen that the intensity of the nested comb is slightly enhanced when a THz field is added to the IR laser-pulse trains, and the structure with two high subpeaks and one low subpeak becomes more regular compared with the case of the IR field alone. In Fig. 2(e), the yield of the HHG comb is also increased by nearly two orders of magnitude, and the comb structure becomes more regular and clear compared with the case of the IR field alone, which is particularly similar to the odd harmonic structure shown in Fig. 2(d). To sum up, the frequency-comb structure driven by the IR-THz combined laser field in below-threshold and plateau harmonics, either the main peaks or subpeaks, is very smooth and regular. The number of subpeaks is $N - 2$ regardless of the odd or even orders. In addition, the yield of some harmonics is increased by nearly two orders of magnitude.

To understand the origin of frequency-comb generation via HHG, especially the influence of the THz laser train on the structure of the frequency comb, we analyze the frequency spectral phase of the induced dipole moment, which can be calculated using Eq. (11). The equally spaced discrete of frequency comb generated via HHG are essentially caused by constructive quantum interference resulting from a phase-locked induced dipole moment [38]. In order to observe the coherent structure of the harmonic phases more precisely, we select four sets of frequency-comb structures around the fifth harmonic (5H) and the ninth harmonics (9H) for the exploration of the coherence; these harmonics are located at low order and in the plateau region, respectively. Figures 3(a) and 3(b) show a comparison of the comb structure and spectral

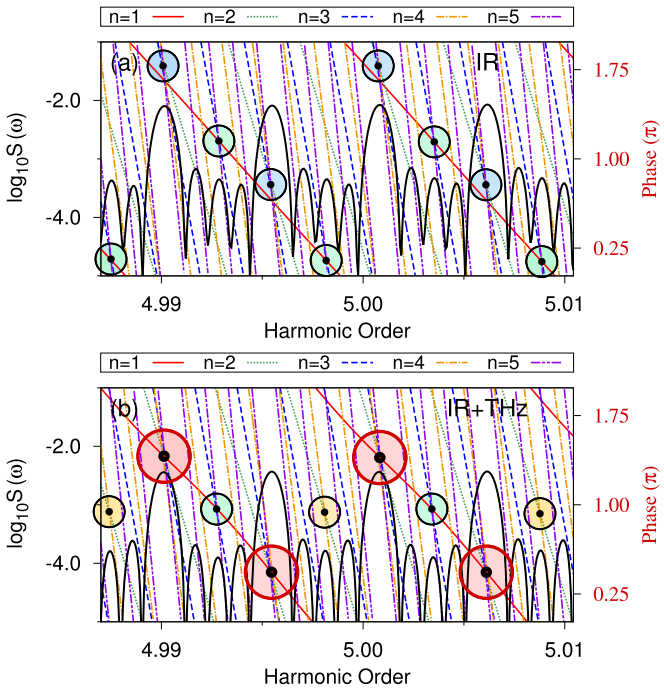

FIG. 3. Spectral phases for the vicinity of the fifth harmonic (5H) located in the below-threshold region in the case of (a) an IR laser-pulse train alone and (b) an IR-THz combined laser-pulse train. The red solid lines represent the harmonic phases for the first pulse ($n = 1$), the green dotted lines are for $n = 2$, the blue dashed lines are for $n = 3$, the yellow dash-dotted lines are for $n = 4$, and the violet short-dashed lines are for $n = 5$. Large red-filled circles indicate complete intersections of all five phases, and small circles indicate partial intersections. The laser parameters used are the same as those in Fig. 1.

phases calculated from the induced dipole moments at 5H for the IR laser train and the IR-THz combined laser field, respectively. The red solid lines represent phases for the first dipole pulse ($n = 1$), the green dotted lines are for $n = 2$, the blue dashed lines are for $n = 3$, the yellow dash-dotted lines are for $n = 4$, and the violet short-dashed lines are for $n = 5$. The large red-filled circles represent all five phases intersecting completely; the harmonic phases are fully coherent. Small circles indicate partial intersections: the blue-, green-, and yellow-filled circles represent the coherence of four, three, and two dipole phases, respectively. The used laser parameters are the same as in Fig. 1. It can be seen that in Fig. 3(a), in the case of the IR field alone, although the comb structure near fifth order is relatively clear, the five spectral phases at the main peak are not fully coherent, so the overall comb-structure regularity is affected. Note that the intensities of the adjacent main peaks in Fig. 3(a) have a slight difference between the complete phase coherence and the quasiphase coherence. However, in Fig. 3(b), by adding a THz laser field, the phase coherence of the main peaks and subpeaks of the frequency comb show good regularity, which is one of the key reasons for improving the coherent synchronization of spectral phases, thus greatly modulating the regularity of the nested frequency-comb structure. Figures 4(a) and 4(b) show a comparison of the structure and spectral phase of the comb

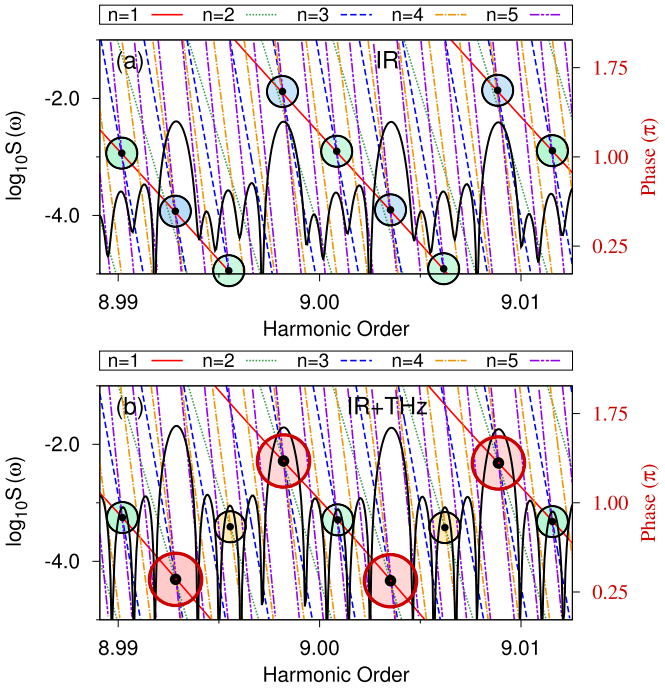

FIG. 4. Spectral phases in the case of (a) an IR laser-pulse train alone and (b) an IR-THz combined laser-pulse train located near the ninth harmonic (9H) of the plateau region. The large red-filled circles indicate that all five phases intersect completely. The other details are consistent with Fig. 3.

at 9H located in the plateau region of the IR laser train and the IR-THz combined laser field, respectively. Figure 4 presents a comparison result similar to that shown in Fig. 3. In contrast, in Fig. 4(b), the dipole phases at the main peak position are more coherent for each pulse, and the coherent positions of the adjacent central subpeaks have good regularity, almost all on the same horizontal line.

It is well known that ionization probability plays a very important role in HHG processes, so we also perform a calculation of the ionization probability between the IR field alone and the IR-THz combined field. In Fig. 5, the purple line with points represents the ionization probability of the IR field alone, and the green solid line represents the ionization

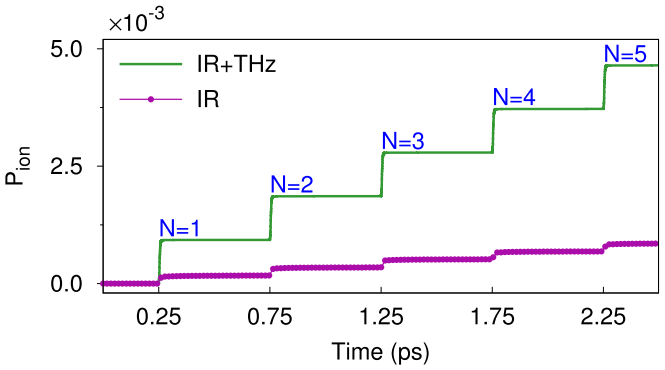

FIG. 5. Ionization probability driven by the IR-THz combined laser field and the IR laser field alone. The laser parameters used are the same as those in Fig. 1.

probability for the IR-THz combined field. The ionization probability can be calculated by

$$P_{\text{ion}}(t) = 1 - \langle \psi(\mathbf{r}, t) | \psi(\mathbf{r}, t) \rangle. \tag{12}$$

It can be found that both of them show the same step for each of their five pulses, which induces a synchronized change in phases, resulting in constructive coherence. The ionization probability of the laser field combined with the THz field is more than 5 times higher than that of the IR laser field alone and exhibits relatively rapid ionization and uniform ionization efficiency. This is because the THz pulse train breaks the symmetry of the IR laser field and greatly enhances the positive amplitudes of the combined field, so the ionization probability is increased, and the ionization becomes faster and more uniform.

According to the semiclassical model, ionization is the first step in HHG of an atom driven by laser fields. That is to say, the laser field is responsible for the ionization regime. This implies that IR and IR combined with a THz field lead to different ionization regimes, and there is an obvious contrast in the ionization probability. We know that the different ionization regimes are related to different quantum channels in HHG. These quantum channels are typically classified by the dynamical phases. To explore the relationship between the features of quantum channels related to the ionization regime and the constructive coherence of the dynamical phase, we discuss the emission properties by calculating the time profile and dynamical phase of the specific harmonic in the below-threshold and plateau regions; we discuss the emission properties by calculating the time profile and dynamical phase of the specific harmonic in the below-threshold and plateau regions. The specific harmonic time profile can be obtained via the wavelet transform [39]:

$$d_{\omega_k}(t_e) = \left| d_{\omega_k}(t_e) \right| \exp\left[-i(\phi_k(t_e) + \omega_k t_e) \right], \tag{13}$$

and the corresponding dynamical phase $\phi_k(t_e)$ can be extracted. As can be seen in Figs. 6(a)–6(j), at the fifth harmonic in the below-threshold region, the efficiency of the harmonic emission peaks generated by the combined field assisted by the THz pulse is almost the same as that of the infrared field alone, so the intensity of the comb main peak is almost the same. However, the two main emission peaks, which are not completely consistent for each pulse, become four almost identical high emission peaks through the modulation of the THz field. Correspondingly, from the dynamical phase corresponding to the emission peak, it can be seen that the synthesized field has only one similar quantum channel where the phase difference is fully locked compared to the case of only IR field. The addition of the THz field greatly improves the synchronization of the harmonic emission, leading to the constructive coherence of the dipole phase and hence optimizing the frequency-comb structure. Similarly, as can be seen from Figs. 7(a)–7(j), the addition of THz field at the ninth harmonic in the plateau region improves the concentration and intensity of the harmonic emission, modulates the messy dynamical phase channels into two completely locked channels, and realizes the optimization of the frequency-comb structure shown in Fig. 1(d). The origin of two completely locked channels comes from the different ionization regime of atoms driven by the IR combined with the THz field. Generally,

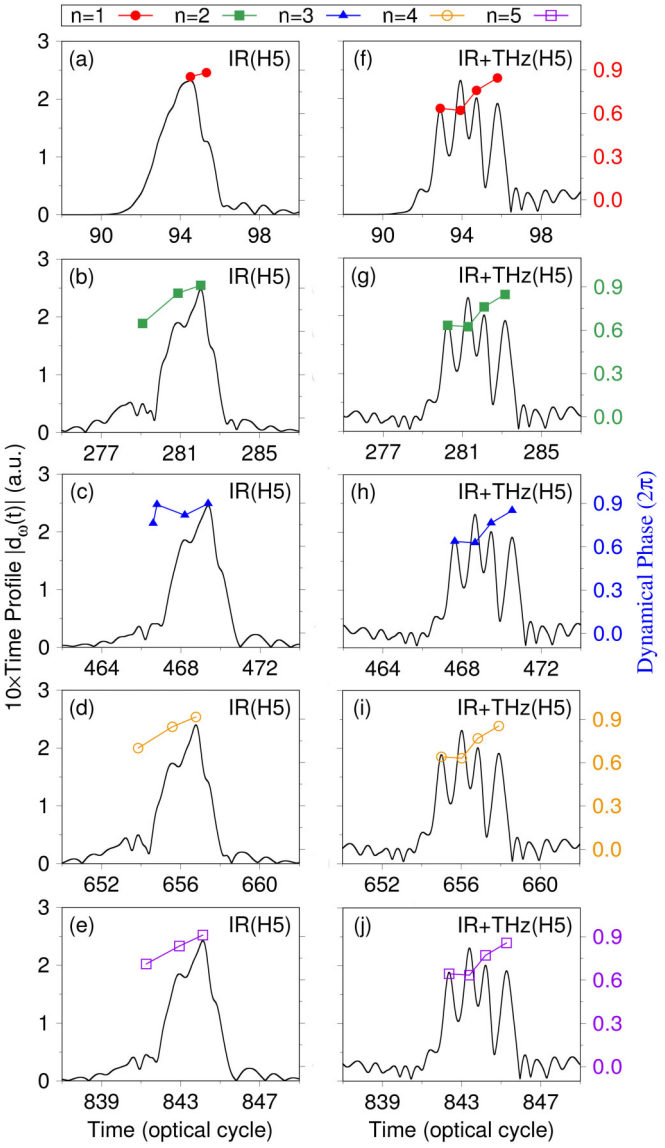

FIG. 6. Comparison of the time profiles (solid black lines) and dynamic phases at the fifth harmonic of (a)–(e) single infrared laser pulses and (f)–(j) the combined laser pulses. The laser parameters are the same as in Fig. 1.

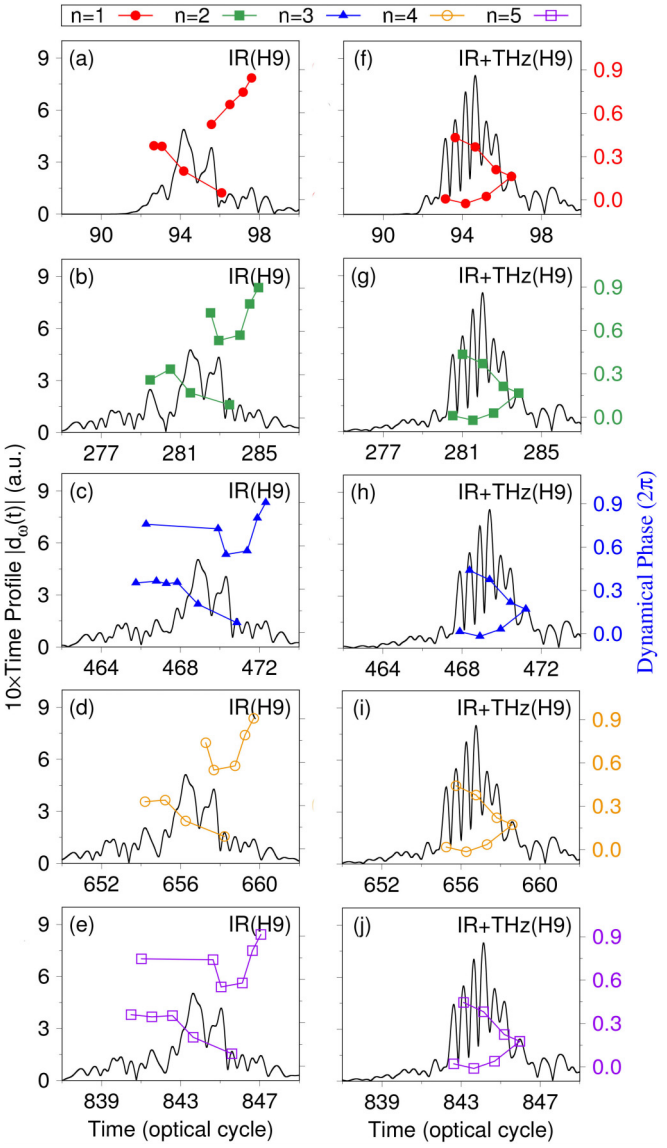

FIG. 7. Comparison of the time profiles (solid black lines) and dynamic phases at the ninth harmonic of (a)–(e) single infrared laser pulses and (f)–(j) the combined laser pulses. The laser parameters are the same as in Fig. 1.

there is one channel below the ionization potential due to the dominant multiphoton ionization, but there are two channels called short and long trajectories in the plateau region due to the dominant tunnel ionization. Therefore, these channels are present in the ninth harmonic but not in the fifth harmonic. In summary, it can be seen from the harmonic emission characteristics that the addition of THz field makes the harmonic emission more efficient and concentrated, thus improving the ionization probability and the intensity corresponding to the frequency comb. As a result, the optimization of the quantum channels shown by the corresponding dynamical phases at the emission peak greatly enhances the harmonic phase synchronization, thus making the structure of the frequency comb more regular.

As discussed above, the ionization probability plays an important role in the frequency comb via HHG. Next, we discuss the influence of the combination of the IR laser field and THz laser field with different frequencies on the structure and intensity of the frequency comb. In Fig. 8, we compare the HHG spectra of the given IR laser field combined with a 25-THz laser field and a 20-THz laser field, and the corresponding results are represented by the green dotted line and red solid line, respectively. The other laser-field parameters are the same as in Fig. 1, except that the THz frequency is changed. It can be seen that both the fourth even harmonics in Fig. 8(b) and the ninth odd harmonics in Fig. 8(c) indicate that the intensity and structure of the frequency combs do not change significantly when the central frequency of the THz field changes slightly. The structures of the main peaks and subpeaks of the frequency comb are very smooth and regular in the below-threshold and plateau harmonics, and the number of subpeaks of the frequency comb is $N-2$ regardless of the

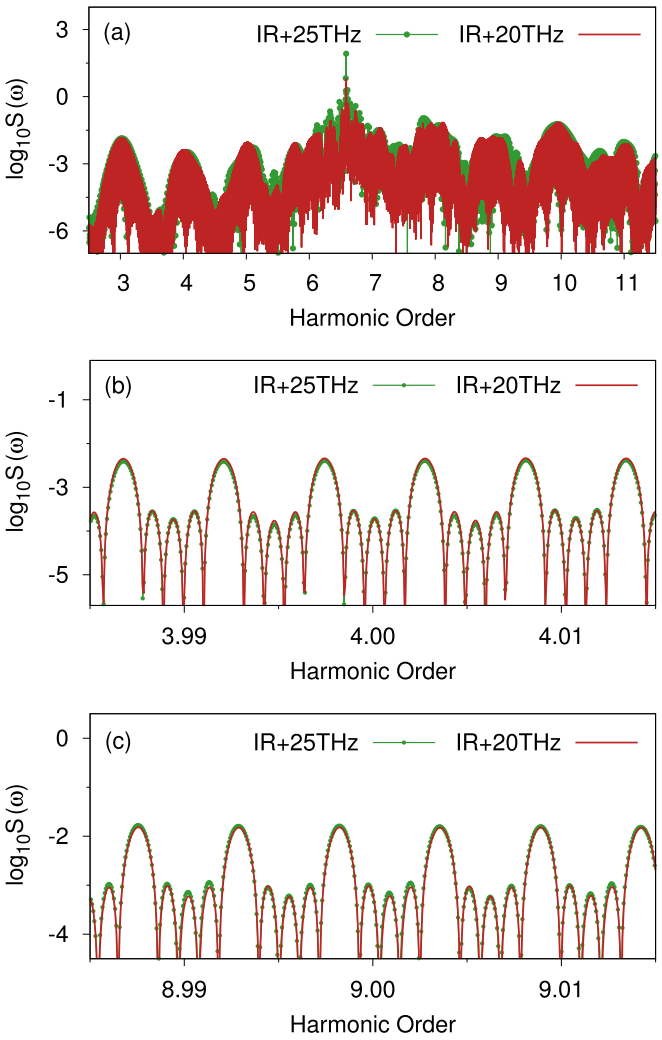

FIG. 8. (a) Comparison of HHG spectra of the given IR laser field combined with 25-THz and 20-THz laser fields. Detailed views of the nested comb structures of the HHG spectra in the vicinity of (b) the fourth harmonic and (c) the ninth harmonic. The other laser parameters used are the same as in Fig. 1.

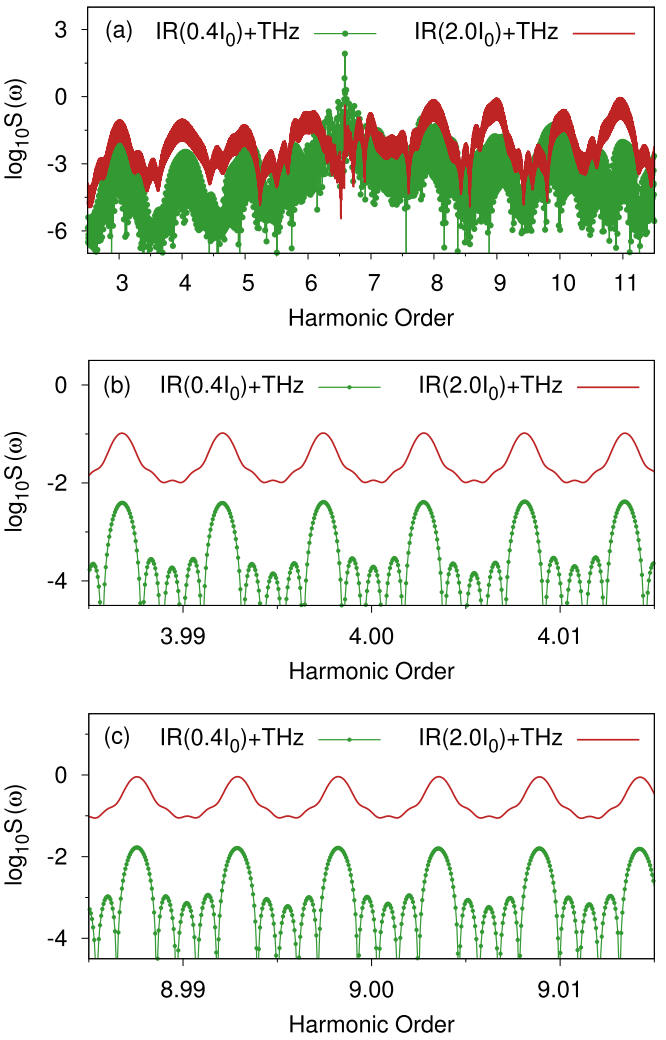

FIG. 9. (a) Comparison of HHG spectra of the given THz laser field combined with the IR laser field with laser intensities $0.4I_0$ and $2.0I_0$ with a 25-THz train. Detailed views of the nested comb structures in the vicinity of (b) the fourth harmonics and (c) the ninth harmonics. The other laser parameters used are the same as in Fig. 1.

odd or even order in the case of both the 25-THz field and the 20-THz field.

To clarify the sensitivity of the frequency-comb structure associated with the laser intensity of laser-pulse trains, we compare the frequency combs via HHG produced in the low-intensity regime and high-intensity regime. Figure 9(a) represents the HHG spectra driven by the infrared laser field for laser intensities $0.4I_0$ ($I_0 = 1.0 \times 10^{14}$ W/cm^2) and $2.0I_0$ with 25-THz laser pulse trains. The field amplitudes of the THz fields of the two combined laser-pulse trains are 1/4 that of the infrared field; that is, when the intensity of the infrared laser field is $0.4I_0$ and $2.0I_0$, the intensity of the THz field is 2.5×10^{12} and 1.25×10^{13} W/cm^2. In Figs. 9(b) and 9(c), detailed views of the nested comb structures in the vicinity of the fourth harmonics and the ninth harmonics are presented. We find that the main peak of the comb structure remains regular, while the subpeaks almost disappear when the ionization is pushed from the low-intensity regime into and high-intensity regime. This result indicates that the ionization regime plays an important role in the frequency comb via HHG.

Figure 10(a) shows the ionization probabilities corresponding to Fig. 8. The results show that the ionization probability reaches almost half of the total number of electrons after the first laser pulse starts, while the ionization probability of the subsequent laser pulse drops sharply to about half of the previous one. The overall ionization probability at this high intensity shows exponential decay. This is because the high laser intensity causes the ground-state population of electrons to be partially depleted at the beginning of the laser-pulse trains, leading to the ionization probability becoming smaller and smaller. As a result, it is hard for the electron to detach from later laser-pulse trains [38]. The analysis of the comb structure and ionization probability under different ionization regimes shows that the change in ionization probability caused by the laser intensity is responsible for the change in the frequency-comb structure. To determine the influence of THz laser pulses with the same intensity but different frequencies

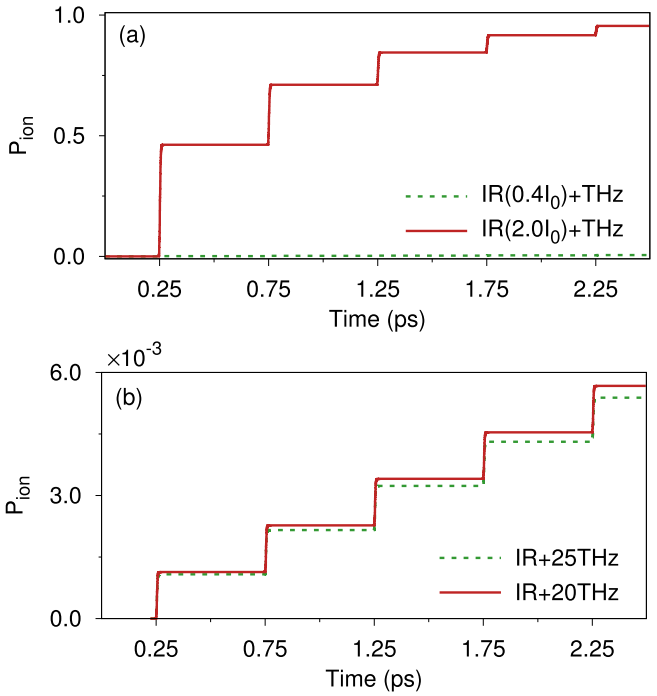

FIG. 10. The corresponding ionization probabilities of Figs. 8 and 9. (a) Ionization probability of the combined laser train for IR laser intensities $0.4I_0$ and $2.0I_0$. (b) Ionization probability of the IR laser train modulated by the 25-THz laser pulse and 20-THz laser pulse.

on the ionization regime, the ionization probabilities of infrared laser trains modulated by 25-THz laser pulses (green dotted line) and 20-THz laser pulses (red solid line) in Fig. 9 are given. As shown in Fig. 10(b), since the change in THz pulse frequency has no dramatic effect on the optical cycle intensity near the maximum peak value of the combined field, the ionization probability of the two cases is less affected by the THz laser-pulse train, so the intensity and structure of the frequency comb are consistent. The above results indicate that the frequency comb of the combined laser train is more regular and the conversion efficiency is higher because the THz laser field optimizes the pulse shape of the combined laser field, rather than simply increasing the intensity.

IV. CONCLUSION

In summary, we proposed a method to modulate the frequency comb by using THz laser-field trains, which optimized the structure of the frequency comb extremely well and improved the comb intensity effectively. The results show that the extra THz laser field greatly breaks the symmetry of the positive and negative components of the laser field, which greatly increases the ionization probability, induces the enhancement of even harmonics generation, and leads to the enhancement of the frequency-comb intensity and the extension of the effective HHG spectra width. Moreover, due to the influence of the IR-THz laser-pulse train on the electron emission trajectory, the efficiency of ionization probability is more rapid and uniform, which improves the synchronization of the dipole phase, thus leading to excellent constructive coherence, and the stability and regularity of the frequency-comb structure generated via HHG are greatly improved. We compared the comb spectra generated at different THz central frequencies and different ionization regions. When the intensity of the combined field is greatly increased, the ionization probability of each pulse is no longer uniform, and the subpeak of the regular comb structure generated by phase interference almost disappears. In addition, the uniformity of the ionization probability of the combined field is not greatly affected when the THz field center frequency is reduced, and the THz center frequency is not restricted to a small interval when using the THz field to optimize the IR field for better comb spectra. These results suggest that the regular structure of the frequency comb is related to the coherence of the phase constructive coherence resulting from the uniformity of the ionization probability induced by the pulse shape of the combined laser train modulated by the THz laser field. Although our results are for the single-atom case, the insights obtained are quite general and are also applicable for understanding the dynamical origin of coherent enhancement of a frequency comb modulated by a terahertz laser field in HHG. According to our previous work [40], the commonly used single-atom model can be sufficient for the proper description of the HHG because the characteristics of the dominant-trajectory electron emission in the single-atom response are not changed after macroscopic propagation. Our results suggest a potential method for generating high conversion efficiency and regular frequency combs, providing a potential method for controlling the generation of XUV and VUV frequency combs.

ACKNOWLEDGMENT

This work was supported by the National Natural Science Foundation of China (Grant No. 12074239).

[1] L. Consolino, M. Nafa, F. Cappelli, K. Garrasi, F. P. Mezzapesa, L. Li, A. G. Davies, E. H. Linfield, M. S. Vitiello, P. De Natale, and S. Bartalini, Nat. Commun. **10**, 2938 (2019).
[2] A. Cingöz, D. C. Yost, T. K. Allison, A. Ruehl, M. E. Fermann, I. Hartl, and J. Ye, Nature (London) **482**, 68 (2012).
[3] N. Picqué and T. W. Hänsch, Nat. Photonics **13**, 146 (2019).
[4] S. T. Cundiff and J. Ye, Rev. Mod. Phys. **75**, 325 (2003).
[5] T. Fortier and E. Baumann, Commun. Phys. **2**, 153 (2019).
[6] S. A. Diddams, D. J. Jones, J. Ye, S. T. Cundiff, J. L. Hall, J. K. Ranka, R. S. Windeler, R. Holzwarth, T. Udem, and T. W. Hänsch, Phys. Rev. Lett. **84**, 5102 (2000).
[7] Q. Y. Lu, F. H. Wang, D. H. Wu, S. Slivken, and M. Razeghi, Nat. Commun. **10**, 2403 (2019).
[8] M. Zimmermann, C. Gohle, R. Holzwarth, T. Udem, and T. W. Hänsch, Opt. Lett. **29**, 310 (2004).
[9] Y. Ma, Y. Z. Ma, Z. Q. Zhou, C. F. Li, and G. C. Guo, Nat. Commun. **12**, 2381 (2021).
[10] H. Jans and X. Rottenberg, Spectrosc. Eur. **34**, 22 (2022).

[11] T. Steinmetz, T. Wilken, C. Araujo-Hauck, R. Holzwarth, T. W. Hänsch, L. Pasquini, A. Manescau, S. D'Odorico, M. T. Murphy, T. Kentischer, W. Schmidt, and Th. Udem, Science **321**, 1335 (2008).
[12] M. J. Yu, Y. Okawachi, A. G. Griffith, M. Lipson, and A. L. Gaeta, Optica **3**, 854 (2016).
[13] A. B. Matsko, A. A. Savchenkov, W. Liang, V. S. Ilchenko, D. Seidel, and L. Maleki, Opt. Lett. **36**, 2845 (2011).
[14] Y. K. Chembo, Nanophotonics **5**, 214 (2016).
[15] A. Rueda, F. Sedlmeir, M. Kumari, G. Leuchs, and H. G. L. Schwefel, Nature (London) **568**, 378 (2019).
[16] C. Gohle, T. Udem, M. Herrmann, J. Rauschenberger, R. Holzwarth, H. A. Schuessler, F. Krausz, and T. W. Hänsch, Nature (London) **436**, 234 (2005).
[17] R. J. Jones, K. D. Moll, M. J. Thorpe, and J. Ye, Phys. Rev. Lett. **94**, 193201 (2005).
[18] M. Nisoli, P. Decleva, F. Calegari, A. Palacios, and F. Martín, Chem. Rev. **117**, 10760 (2017).
[19] T. Popmintchev, M. C. Chen, D. Popmintchev, P. Arpin, S. Brown, S. Ališauskas, G. Andriukaitis, T. Balčiunas, O. D. Mücke, A. Pugzlys, A. Baltuška, B. Shim, S. E. Schrauth, A. Gaeta, C. Hernández-García, L. Plaja, A. Becker, A. Jaron-Becker, M. M. Murnane, and H. C. Kapteyn, Science **336**, 1287 (2012).
[20] P. B. Corkum, Phys. Rev. Lett. **71**, 1994 (1993).
[21] D. C. Yost, T. R. Schibli, J. Ye, J. L. Tate, J. Hostetter, M. B. Gaarde, and K. J. Schafer, Nat. Phys. **5**, 815 (2009).
[22] M. Uiberacker, Th. Uphues, M. Schultze, A. J. Verhoef, V. Yakovlev, M. F. Kling, J. Rauschenberger, N. M. Kabachnik, H. Schröder, M. Lezius, K. L. Kompa, H.-G. Muller, M. J. J. Vrakking, S. Hendel, U. Kleineberg, U. Heinzmann, M. Drescher, and F. Krausz, Nature (London) **446**, 627 (2007).
[23] M. Herrmann, M. Haas, U. D. Jentschura, F. Kottmann, D. Leibfried, G. Saathoff, C. Gohle, A. Ozawa, V. Batteiger, S. Knünz, N. Kolachevsky, H. A. Schüssler, T. W. Hänsch, and Th. Udem, Phys. Rev. A **79**, 052505 (2009).
[24] W. G. Rellergert, D. DeMille, R. R. Greco, M. P. Hehlen, J. R. Torgerson, and E. R. Hudson, Phys. Rev. Lett. **104**, 200802 (2010).
[25] D. Z. Kandula, C. Gohle, T. J. Pinkert, W. Ubachs, and K. S. E. Eikema, Phys. Rev. Lett. **105**, 063001 (2010).
[26] J. J. Carrera, S. K. Son, and S.-I. Chu, Phys. Rev. A **77**, 031401(R) (2008).
[27] C. T. Liang, Y. Y. Wu, Z. B. Wang, and P. C. Li, Opt. Express **30**, 2413 (2022).
[28] S. S. Dhillon, M. S. Vitiello, E. H. Linfield, A. G. Davies, M. C. Hoffmann, J. Booske, C. Paoloni, M. Gensch, P. Weightman, G. P. Williams, E. Castro-Camus, D. R. S. Cumming, F. Simoens, I. Escorcia-Carranza, J. Grant, S. Lucyszyn, M. Kuwata-Gonokami, K. Konishi, M. Koch, C. A. Schmuttenmaer *et al.*, J. Phys. D **50**, 043001 (2017).
[29] D. Burghoff, T. Y. Kao, N. Han, C. W. I. Chan, X. W. Cai, Y. Yang, D. J. Hayton, J. R. Gao, J. L. Reno, and Q. Hu, Nat. Photonics **8**, 462 (2014).
[30] H. A. Hafez, S. Kovalev, J. C. Deinert, Z. Mics, B. Green, N. Awari, M. Chen, S. Germanskiy, U. Lehnert, J. Teichert, Z. Wang, K.-J. Tielrooij, Z. Y. Liu, Z. P. Chen, A. Narita, K. Müllen, M. Bonn, M. Gensch, and D. Turchinovich, Nature (London) **561**, 507 (2018).
[31] J. A. Fülöp, Z. Ollmann, C. Lombosi, C. Skrobol, S. Klingebiel, L. Pálfalvi, F. Krausz, S. Karsch, and J. Hebling, Opt. Express **22**, 20155 (2014).
[32] K. Kovács, E. Balogh, J. Hebling, V. Toşa, and K. Varjú, Phys. Rev. Lett. **108**, 193903 (2012).
[33] M. Beck, H. Schäfer, G. Klatt, J. Demsar, S. Winnerl, M. Helm, and T. Dekorsy, Opt. Express **18**, 9251 (2010).
[34] A. Sell, A. Leitenstorfer, and R. Huber, Opt. Lett. **33**, 2767 (2008).
[35] X. M. Tong and S. I. Chu, Chem. Phys. **217**, 119 (1997).
[36] O. Schubert, M. Hohenleutner, F. Langer, B. Urbanek, C. Lange, U. Huttner, D. Golde, T. Meier, M. Kira, S. W. Koch, and R. Huber, Nat. Photonics **8**, 119 (2014).
[37] A. D. Koulouklidis, C. Gollner, V. Shumakova, V. Yu. Fedorov, A. Pugžlys, A. Baltuška, and S. Tzortzakis, Nat. Commun. **11**, 292 (2020).
[38] J. J. Carrera and S.-I. Chu, Phys. Rev. A **79**, 063410 (2009).
[39] X. M. Tong and S.-I. Chu, Phys. Rev. A **61**, 021802(R) (2000).
[40] P. C. Li and S.-I. Chu, Phys. Rev. A **86**, 013411 (2012).